



Antitumor Activity of Chitosan-Coated Iron Oxide Nanocomposite Against Hepatocellular Carcinoma in Animal Models

Monda M. M. Badawy¹ · Gehan R. Abdel-Hamid² · Hebatallah E. Mohamed²

Received: 22 February 2022 / Accepted: 28 March 2022 / Published online: 22 July 2022
© The Author(s) 2022

Abstract

Hepatocellular carcinoma (HCC) is among the most prevalent and lethal cancers worldwide. Chitosan-coated iron oxide nanocomposite ($\text{Fe}_3\text{O}_4/\text{Cs}$) is a promising bio-nanomaterial for many biological applications. The objective of this research was to evaluate the anticancer efficacy of $\text{Fe}_3\text{O}_4/\text{Cs}$ against HCC in animal models. Fe_3O_4 nanoparticles were prepared and added to chitosan solution; then, the mixture was exposed to gamma radiation at a dose of 20 kGy. Rats have received diethylnitrosamine (DEN) orally at a dose of 20 mg/kg body weight 5 times per week during a period of 10 weeks to induce HCC and then have received $\text{Fe}_3\text{O}_4/\text{Cs}$ intraperitoneal injection at a dose of 50 mg/kg body weight 3 times per week during a period of 4 weeks. After the last dose of $\text{Fe}_3\text{O}_4/\text{Cs}$ administration, animals were sacrificed. DEN induced upregulation of PI3K/Akt/mTOR and MAPK (ERK, JNK, P38) signaling pathways and inflammatory markers (TLR4, iNOS, and TNF- α). DEN also decreases cleaved caspase-3 and increases liver enzymes (ALT, AST, and GGT) activities. Administration of $\text{Fe}_3\text{O}_4/\text{Cs}$ significantly ameliorated the above-mentioned parameters.

Keywords Hepatocellular carcinoma · Iron oxide nanocomposite · Gamma radiation · PI3K/Akt/mTOR · MAPK

Introduction

Hepatocellular carcinoma (HCC) is the most prevalent primary liver cancer and the fourth highest cause of cancer-related death worldwide [1]. HCC usually with poor prognosis. Over the previous few decades, the number of people diagnosed with HCC and dying from it has grown. Advanced HCC, on the other hand, has very few therapy choices [2]. Chemotherapy is the most common traditional cancer treatment, rather than local lesions that can be treated with surgery or radiotherapy. Anticancer medications, on

the other hand, come with many negative side effects. Each medicine has its own set of side effects that might lead to patient noncompliance and a decline in quality of life. The production of reactive oxygen species (ROS) is one of the most common causes of unfavorable responses [3].

Recent advances in nanotechnology have provided a plethora of methods for fighting cancer with novel and effective therapeutic agents that avoid the drawbacks that standard medications have. Nanomaterials have been used as cancer therapeutics due to their ability to modulate autophagy [4]. Many research findings have shown that nanomaterials, particularly metallic nanoparticles, could be used to treat cancer by promoting a variety of events such as mitochondrial damage, lysosome impairment, endoplasmic reticulum stress, and signalling pathway alterations, which all result in mitophagy stimulation, oxidative stress, and autophagic cell death. Importantly, as compared to noncancerous cells, metallic nanoparticles have shown intrinsic selectivity in triggering autophagy in cancer cells. Metal-based nanomaterials, on the other hand, may play conflicting roles in cell fate, inducing pro-survival autophagy in both cancer and normal cells [5–7]. As a result, inhibiting autophagy could be a realistic strategy for improving cancer therapy efficacy. Magnetic iron oxide nanoparticles (Fe_3O_4 NPs) are a type

✉ Monda M. M. Badawy
monda.badawy@eaea.org.eg; mondabadawy@gmail.com

Gehan R. Abdel-Hamid
gehan.abdel-hamid@eaea.org.eg

Hebatallah E. Mohamed
hebatallah.mohamed@eaea.org.eg

¹ Department of Health Radiation Research, National Center for Radiation Research and Technology (NCRRT), Egyptian Atomic Energy Authority (EAEA), Cairo, Egypt

² Department of Radiation Biology, National Center for Radiation Research and Technology (NCRRT), Egyptian Atomic Energy Authority (EAEA), Cairo, Egypt

of multifunctional nanomaterial that is increasingly being used in a variety of biomedical fields, such as magnetic resonance imaging, magnetic hyperthermia, magnetic targeting, magnetic separation, biological catalysis, photo-responsive therapy, and drug delivery. They are currently widely used in tumor diagnosis and treatment [8]. Because of its low toxicity in biological systems, iron oxide nanoparticles have shown considerable promise in biomedical applications. Iron oxide nanoparticles' magnetic and semiconductor characteristics may also lead to multifunctional medical uses [9]. Other advantages of Fe₃O₄ NPs include prolonged blood circulation, rapid clearance, low side effects, good imaging, and therapeutic efficacy [10]. The key advantage of these nanoparticles over conventional drug delivery systems is their excellent biodistribution in the body [9]. Furthermore, Fe₃O₄ NPs have catalytic activity similar to peroxidase and have been proposed as a mimic enzyme for cancer therapy via the well-known Fenton reactions, which can catalyze endogenous hydrogen peroxide (H₂O₂) into the hydroxyl radical (•OH) with high cytotoxicity and cause tumor cell death [11].

Chitosan is reported to have a high biodegradability, biocompatibility, and stability, as well as minimal toxicity and immunogenicity in cells [12]. Chitosan is also a mucoadhesive cationic polymer that has been used widely in recent years to deliver anticancer chemotherapeutics to tumor cells [13]. Chitosan's amine group will promote solubility and hemocompatibility in the intracellular environment [12]. Furthermore, the positive surface of nanoparticles will interact with many cellular components, which is a characteristic of chitosan, resulting in a longer connection between the encapsulated component and the cells. The presence of chitosan on the particle surface may also aid in the opening of tight intracellular junctions, thereby increasing cellular absorption and hence therapeutic efficiency [14, 15]. Fe₃O₄/Cs has potentially better biomedical properties than uncoated Fe₃O₄ NPs; thus, it is a promising bio-nanomaterial for many biological applications [16].

The actions of the phosphatidylinositol 3 kinase/kinase Akt/mammalian target of rapamycin (PI3K/Akt/mTOR) pathways trigger autophagy. mTOR is a master regulator of cellular metabolism that responds to a variety of extracellular cues such as nutrition, growth hormones, and stress [17]. Its signalling pathway starts with insulin-activating PI3K, then moves on to Akt, which then activates mTOR [18]. Changes in cellular pathway proteins like PI3K/Akt/mTOR and MAPK/ERK, which are extensively dysregulated in malignant tumors, also support malignant cells' ability to avoid apoptotic death and contribute to chemotherapy resistance [19]. Various types of NPs have been found to influence components in the mTOR signalling pathway and other related pathways, such as the AMPK and ERK pathways [20].

Towards this purpose, Fe₃O₄/Cs was successfully prepared and evaluated as anticancer against HCC in animal models.

Material and Methods

Materials

Diethylnitrosamine (DEN) purchased from Sigma-Aldrich (cat# N0756, St. Louis, MO, USA). Chitosan, ferrous chloride tetrahydrate (FeCl₂ · 4H₂O), ferric chloride hexahydrate (FeCl₃ · 6H₂O), and A sodium hydroxide (NaOH) were purchased from Merck. All chemicals were guaranteed or analytical grade reagents commercially available and used without further purification.

Preparation of Fe₃O₄ Nanoparticles Coated with Chitosan

Fe₃O₄ nanoparticles were prepared by co-precipitating the Fe³⁺ and Fe²⁺ ions by, firstly, dissolving 4 gm of (FeCl₃ · 6H₂O) and 2 gm of (FeCl₂ · 4H₂O) in 200 ml of doubly distilled water by vigorous stirring on magnetic stirrer; then 200 ml of sodium hydroxide (0.5 M) was added drop wisely and very slowly under stirring and heating to 80 °C until complete precipitation obtained [21]. Heating was continued at 80° for another 30 min, and then dispersion of formed magnetic nanoparticles washed several times with water by decantation to remove any excess sodium hydroxide. One hundred milliliter of the prepared Fe₃O₄ nanodispersion was added to 100 ml of chitosan solution at a concentration of 1% wt/v and vigorously stirred under heating at 80 °C for 1 h; then the mixture exposed to gamma radiation at a dose of 20 kGy. The formed magnetic nanoparticles that coated with chitosan exposed to gamma radiation to initiate partial degradation of chitosan chains and to facilitate the coating process of Fe₃O₄ NPs by chitosan.

Characterizations of Fe₃O₄/Chitosan Nanodispersions

Transmission Electron Microscopy (TEM)

TEM was used to observe the morphology (size and shape) of the formed magnetic nanoparticles. A drop of the resultant dispersion of magnetic nanoparticles mixture was deposited on an ultrathin carbon supported Cu grid and air-dried. Energy-filtered electron powder diffraction used TEM JEOL: JEM-100cx.

The X-Ray Diffraction (XRD)

The XRD analysis was performed using XD-DI Series, Shimadzu apparatus using nickel-filtered and Cu-K target, available in NCRRT.

Determination of the Median Lethal Dose (LD50) of Fe₃O₄/Cs

Fe₃O₄/Cs were given intraperitoneally to male albino rats in doses ranging from 50 to 700 mg/kg. Mortality after 24 h was registered.

The LD50 of Fe₃O₄/Cs was calculated according to the formula [22].

$$LD50 = Dm - \Sigma(Zxd)/n$$

where *Dm* is the minimum dose which kills all animals in the group; *Z* is the mean of dead animals in two successive groups; *d* is the constant factor between two successive groups; *n* is the number of animals of each group; and Σ is the sum of (*Zxd*).

Experimental Design

Animal Groups

Twenty-four male albino rats (weighing 120–150 g at the start of the experiment) were randomly divided into 4 groups (6 animals/group):

Group 1 (Control): Healthy animals do not receive any treatment.

Group 2 (DEN): Rats were received diethylnitrosamine (DEN) orally at a dose of 20 mg/kg body weight, five times a week during a period of 10 weeks [23].

Group 3 (Fe₃O₄/Cs): Rats were received 50 mg/kg body weight of chitosan-coated iron oxide nanocomposite (Fe₃O₄/Cs) suspended in distilled water by intraperitoneal injection three times a week during a period of 4 weeks [24].

Group 4 (DEN + Fe₃O₄/Cs): Rats were received DEN orally as group 2 then treated with Fe₃O₄/Cs as group 3.

Rats were obtained from the National Centre for Radiation Research and Technology (NCRRT), Cairo, Egypt. The rats were housed in cages and maintained a 12-h light/dark cycle. They were allowed to acclimatize to the environmental conditions for 1 week before starting the experiment and were kept on standard food pellets containing all nutritive elements and liberal water ad libitum. All the ethical

protocols for animal treatment were approved by the Ethical Committee at the National Center for Radiation Research and Technology (no: 3 A/ 22).

After the last dose of Fe₃O₄/Cs administration, rats were fasted overnight. Blood samples were withdrawn from the heart of each animal, under light anesthesia by diethyl ether. Blood was allowed to coagulate and then was centrifuged at 3000 rpm for 15 min, and the serum was separated in another tube. Immediately after blood sampling, animals were sacrificed by cervical dislocation; liver tissues were rapidly removed, washed in ice-cold saline, plotted to dry, and then were kept at – 80 °C till the day of analysis. Another part of liver tissue was placed in 10% formalin prepared in phosphate buffered saline (PBS) to be used for histopathological examination.

Molecular Investigation

Western Immunoblotting Analysis of PI3K/AKT/ mTOR and MAPK (P38, ERK1/2 and JNK) Proteins in Liver Tissue Homogenate Liver tissue protein was extracted using TRIzol reagent, and protein concentration was quantified according to Bradford [25]. Twenty microgram of protein per lane was separated by sodium dodecyl sulfate–polyacrylamide gel electrophoresis (SDS-PAGE) using 10% acrylamide gels and transferred on to PVDA membranes. Membranes were incubated at room temperature for 2 h with blocking solution (5% non-fat dried milk in 10 mMTris-HCl, pH 7.5, 100 mMNaCl, and 0.1% Tween 20) and then incubated overnight at 4 °C with primary antibody towards targeted proteins with β-actin as a control. After washing three times in washing buffer (10 mMTris-HCL, pH 7.5, 100 mMNaCl, and 0.1% Tween 20), membrane was incubated with the secondary monoclonal antibody conjugated to horseradish peroxidase at room temperature for 2 h, and then membranes were washed four times with the same washing buffer. Membrane was developed and visualized by chemiluminescence using Invitrogen™ detection kit (Catalog #AHO1202) according to the manufacturer's protocols and then exposed to X-ray film. Quantification of PI3K/AKT/ mTOR and MAPK (P38, ERK1/2 and JNK) proteins was carried out using scanning laser densitometer (Biomed Instrument Inc., USA).

Determination of Toll-Like Receptor 4 (TLR4) and Inducible Nitric Oxide Synthase (iNOS) Gene Expression Total RNA was extracted from liver tissue using RNeasy Mini Kit (Qiagen, Cat. No. 74104) according to the manufacturer's instructions. First strand complementary DNA (cDNA) synthesis was performed using QuantiTect Reverse Transcription Kit (Qiagen, Cat. No. 205311) according to the manufacturer's instructions using 1 µg RNA as a template. RT-PCR were performed in a thermal cycler step one plus

(Applied Biosystems, USA) using the Sequence Detection Software (PE Biosystems, CA). The oligonucleotides utilized in these experiments are listed in Table 1. The reaction mixture of total volume 25 μ L was consisting of 2X SYBR Green PCR Master Mix (Qiagen, Cat. No. 204143), 900 nM of each primer and 2 μ L of cDNA. PCR thermal-cycling conditions included an initial step at 95 $^{\circ}$ C for 5 min; 40 cycles at 95 $^{\circ}$ C for 20 s, annealing at 52 $^{\circ}$ C or 57 $^{\circ}$ C or 60 $^{\circ}$ C (as in Table 1) for 30 s, and 72 $^{\circ}$ C for 30 s. The relative expression of the real-time reverse transcriptase PCR products was determined by the $\Delta\Delta$ Ct method. This method calculates a relative expression to housekeeping gene using the equation: fold induction = $2^{-(\Delta\Delta Ct)}$, where $\Delta\Delta Ct = Ct$ [gene of interest (unknown sample)]— Ct housekeeping gene (unknown sample)—[Ct gene of interest (calibrator sample)]— Ct housekeeping gene (calibrator sample)] [26].

Biochemical Investigation

Tumor necrosis factor alpha (TNF- α) and cleaved caspase-3 were measured in liver tissue homogenates, according to the manufacturer's instructions using ELISA kits supplied by MyBioSource, Inc. P.O. Box 153,308 San Diego, CA 92,195–3308, USA, while alanine aminotransferase (ALT), aspartate aminotransferase (AST), and gamma-glutamyl transferase (GGT) activities were analyzed in serum using commercial kits provided by Spinreact (Spain).

Histopathological Examination

Liver tissue specimens were fixed in 10% formol saline, then trimmed off, and washed and dehydrated in ascending grades of alcohol. The dehydrated specimens were then cleared in xylene, embedded in paraffin blocks, and sectioned at 4–6 μ m thick. The obtained tissue sections were deparaffinized using xylol and stained using hematoxylin and eosin (H&E) for histopathological examination through the electric light microscope [27].

Histological Grade of Hepatocellular Carcinoma The most widely used grading system in HCC (Edmondson and Steiner

system). Grade I consists of small tumor cells, arranged in trabeculae, with abundant cytoplasm and minimal nuclear irregularity that are almost indistinguishable from normal liver tissue. Grade II tumors have prominent nucleoli, hyperchromatism, and some degree of nuclear irregularity. Grade III tumors show more pleomorphism than grade II and have angulated nuclei. Grade IV tumors have prominent pleomorphism and often anaplastic giant cells.

The pathological response of HCC to therapy was graded as Galal et al. (2013) [28].

Grade	Pathological response
Complete	100% tumor necrosis
Partial	51–99% tumor necrosis
Poor	<50% tumor necrosis

Statistical Analysis

The data were presented as means \pm standard error of mean (S.E.); they were analyzed using one-way ANOVA followed by Tukey–Kramer multiple comparison test. The Graph Prism software, version 5, Inc., USA, was used to perform the statistical analysis and graphical presentations. The level of significance was fixed at $P \leq 0.05$ with respect to all statistical tests.

Results

Characterization of Fe₃O₄/Cs

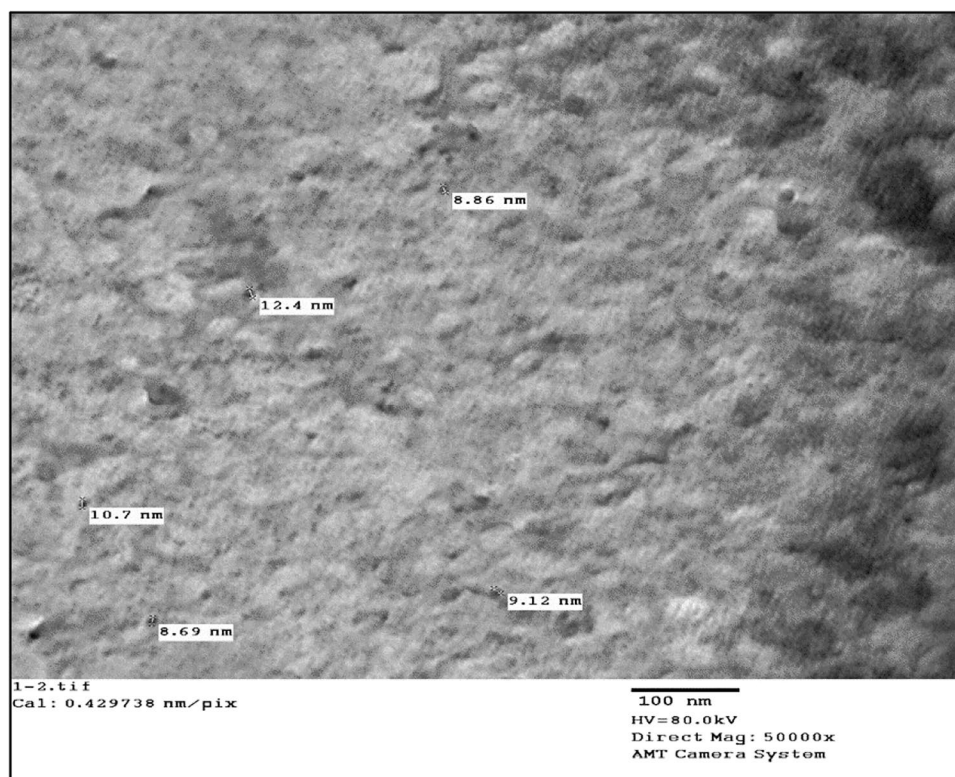
Transmission Electron Microscopy (TEM)

Figure 1 depicts a typical TEM micrograph of Fe₃O₄/chitosan nanoparticles. Because chitosan inhibits nanoparticle aggregation and consequently helped in uniform dispersion of the nanoparticles, Fe₃O₄/chitosan nanoparticles showed virtually little dispersion, with a mean

Table 1 Primer sequences for the genes amplified

Gene	Strand	Sequence 5'—3'	Product length (bp)	Annealing temperature ($^{\circ}$ C)	Ref. Seq
TLR4	F	ATGAGGACTGGGTGAGAAAC	161	52	NM_019178
	R	CACCACCACAATAACTTTCC			
iNOS	F	CTCACTGTGGCTGTGGTCACCTA	101	60	NM_012611
	R	GGGTCTTCGGGCTTCAGGTTA			
β -actin	F	GATCAAGATCATTGCTCCTCCTGA	170	57	NM_031144
	R	CAGCTCAGTAACAGTCCGCCT			

Fig. 1 TEM micrograph for the $\text{Fe}_3\text{O}_4/\text{Cs}$



diameter of about 9.95 nm. This might be due to the reaction taking place exclusively on the surface of the particle, and hence the attempt to make monodispersed Fe_3O_4 /chitosan nanoparticles in this study was successful.

The X-Ray Diffraction (XRD)

Figure 2 shows the XRD of $\text{Fe}_3\text{O}_4/\text{Cs}$, which confirms the formation of Fe_3O_4 /Chitosan nanoparticles through appearance of the characteristic peaks related to Fe_3O_4 nanoparticles at 2-Theta: 35 °C, 42 °C, 58, and 63. The appearance of the broad peak in the 2-Theta range 20–30° is

related to the polymeric part of chitosan. Also, the coating of magnetic nanoparticles with chitosan chains causes a noticeable change in the XRD base line of Fe_3O_4 NPs (Fig. 2).

The Median Lethal Dose (LD50) of $\text{Fe}_3\text{O}_4/\text{Cs}$

The results revealed that the LD50 was found to be 500 mg/kg body weight for the $\text{Fe}_3\text{O}_4/\text{Cs}$ for the intraperitoneal administration (Table 2). One-tenth of the LD50 value has been used as an ideal dose to determine the in vivo antitumor activity of $\text{Fe}_3\text{O}_4/\text{Cs}$.

Fig. 2 the XRD of $\text{Fe}_3\text{O}_4/\text{Cs}$

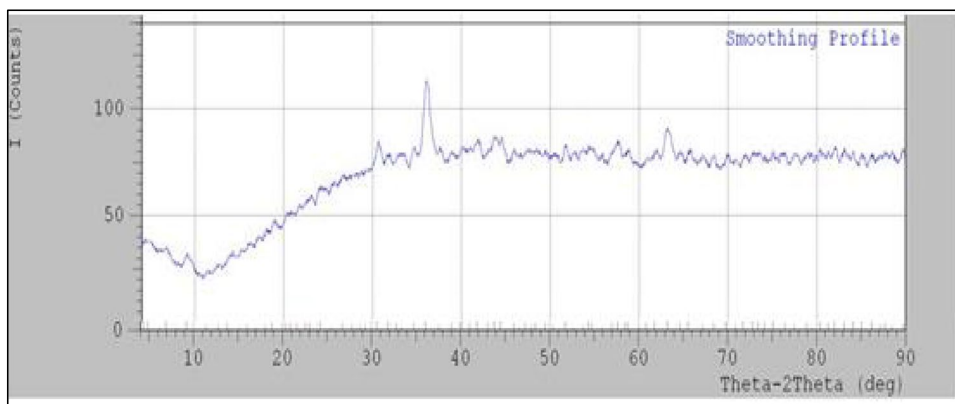


Table 2 Calculation of the median lethal dose (LD50) of Fe₃O₄/Cs

Dose of Fe ₃ O ₄ /Cs (mg/kg body weight)	Number of animals	Number of dead animals	Z	d	(Z) × (d)
50	6	0	0	50	0
100	6	0	0	50	0
200	6	0	0	100	0
300	6	0	0	100	0
400	6	2	1	100	100
500	6	3	2.5	100	250
600	6	4	3.5	100	350
700	6	6	5	100	500

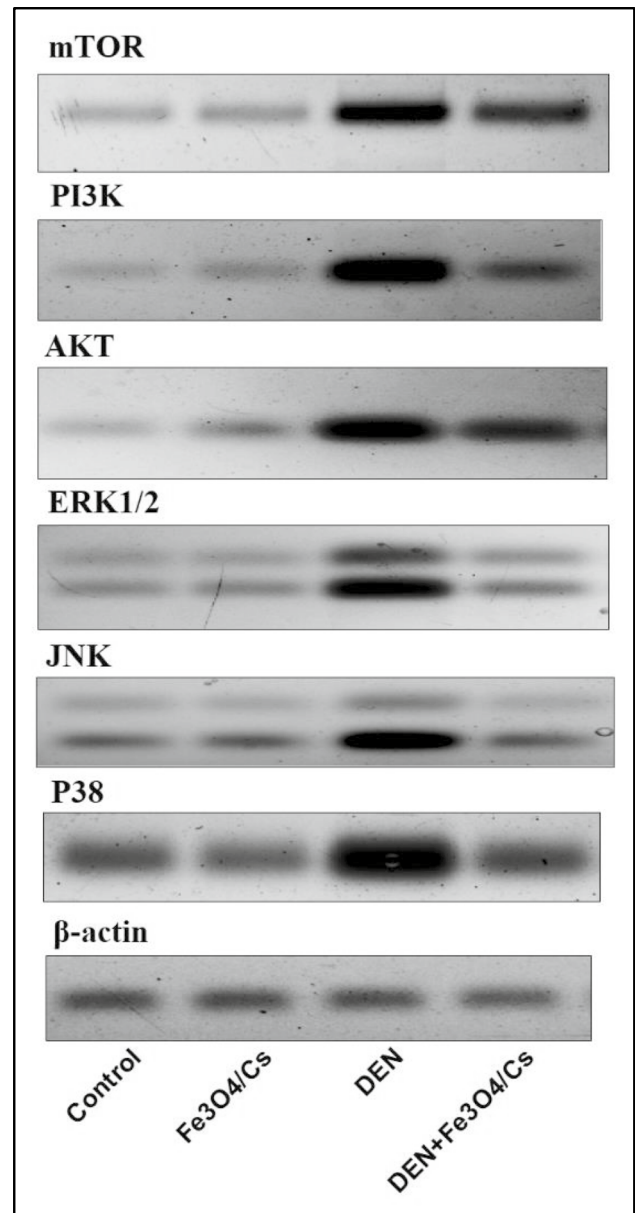
$$LD50 = 700 - (1200/6) = 700 - 200 = 500 \text{ mg/kg}$$

Molecular and Biochemical Studies

The Effect of Fe₃O₄/Cs on PI3K/AKT/ mTOR and MAPK (P38, ERK1/2 and JNK) Pathways

Treatment with DEN manifested a significant ($P \leq 0.05$) increase in the expression of the PI3K, AKT, and mTOR signal pathways (PI3K, 4.2-fold; AKT, 1.9-fold; and mTOR, 3.7-fold in respect to normal control). Treatment with Fe₃O₄/Cs induces a remarkable reduction in the expression of (PI3K, -0.54-fold; AKT, -0.57-fold; and mTOR, -0.53-fold in respect to DEN) as shown in Table 3.

Moreover, protein expression of the mitogen-activated protein kinase (MAPK) family members shows a significant ($P \leq 0.05$) increase (p38 MAPK, 4.08-fold; ERK1/2, 3.88-fold; JNK, 2.51-fold in DEN-treated rats in respect to normal control). Treatment with Fe₃O₄/Cs for DEN + Fe₃O₄/Cs group induces a remarkable reduction in these proteins (p38 MAPK, -0.59-fold; ERK1/2, -0.29-fold; JNK, -0.64-fold in respect to DEN group) as shown in Table 3 and Fig. 3.

**Fig. 3** The effect of Fe₃O₄/Cs on PI3K/AKT/ mTOR and MAPK (P38, ERK1/2 and JNK) protein expression**Table 3** The effect of Fe₃O₄/Cs on PI3K/AKT/ mTOR and MAPK (P38, ERK1/2, and JNK) pathways

	PI3K	AKT	mTOR	P38	ERK1/2	JNK
Control	1.02 ± 0.01	1.02 ± 0.01	1.00 ± 0.04	1.01 ± 0.01	1.04 ± 0.02	1.04 ± 0.04
Fe ₃ O ₄ /Cs	1.03 ± 0.02	1.06 ± 0.03	1.00 ± 0.01	1.04 ± 0.03	1.01 ± 0.01	1.03 ± 0.01
DEN	5.30 ± 0.85 ^a	2.95 ± 0.21 ^a	4.70 ± 0.21 ^a	5.13 ± 0.01 ^a	5.07 ± 0.05 ^a	3.65 ± 0.21 ^a
DEN + Fe ₃ O ₄ /Cs	2.42 ± 0.54 ^b	1.27 ± 0.33 ^b	2.20 ± 0.14 ^{a,b}	2.10 ± 0.42 ^{a,b}	3.55 ± 0.35 ^{a,b}	1.30 ± 0.14 ^b

Each value represents the mean ± standard deviation.

^aSignificant difference versus control group at $P \leq 0.05$.

^bSignificant difference versus DEN group at $P \leq 0.05$.

The Effect of Fe₃O₄/Cs on TLR4, iNOS, TNF- α , and Cleaved Caspase-3

The evaluation for the anti-inflammatory activity of Fe₃O₄/Cs was shown in Fig. 4; the data revealed a high significant ($P \leq 0.05$) increase in the levels of the inflammatory biomarkers, TLR4 and iNOS (5.01-fold and 4.83-fold), respectively, in DEN-treated rats as compared to the corresponding control. In addition, the data displayed a high significant ($P \leq 0.05$) increase in the levels of TNF- α (3.57-fold) with significant decrease in cleaved caspase-3 activity (-0.76 -fold) in DEN-treated rats as compared to the corresponding control. Meanwhile, the data displayed a dramatic decrease in (TLR4, -0.56 -fold; iNOS, -0.76 -fold; TNF- α , -0.51 -fold) with significant increase in the cleaved caspase-3 activity (5.1-fold) for Fe₃O₄/Cs + DEN treatment group as compare to DEN group.

The Effect of Fe₃O₄/Cs on Liver Function Biomarkers

The levels of ALT, AST, and GGT in the serum of all groups were examined to see if Fe₃O₄/Cs had any influence on liver function biomarkers. As shown in Fig. 5, DEN treatment caused severe liver injury, as evidenced by a significant ($P \leq 0.05$) increase in serum (ALT, 3.2-fold; AST, 0.73-fold; and GGT, 6.5-fold for DEN group vs. control group), which was mitigated by Fe₃O₄/Cs treatment (ALT, -0.46 -fold; AST, -0.12 -fold; and GGT, -0.73 -fold for Fe₃O₄/Cs + DEN group vs. DEN group).

Histopathological Observation.

Light microscopic observation for control group demonstrated control hepatic tissue included normal polygonal cells with noticeable round nuclei and eosinophilic

Fig. 4 The effect of Fe₃O₄/Cs on the inflammatory biomarkers (TLR4 and iNOS), TNF- α , and cleaved caspase-3. ^aSignificant difference versus control group at $P \leq 0.05$; ^bsignificant difference versus DEN group at $P \leq 0.05$

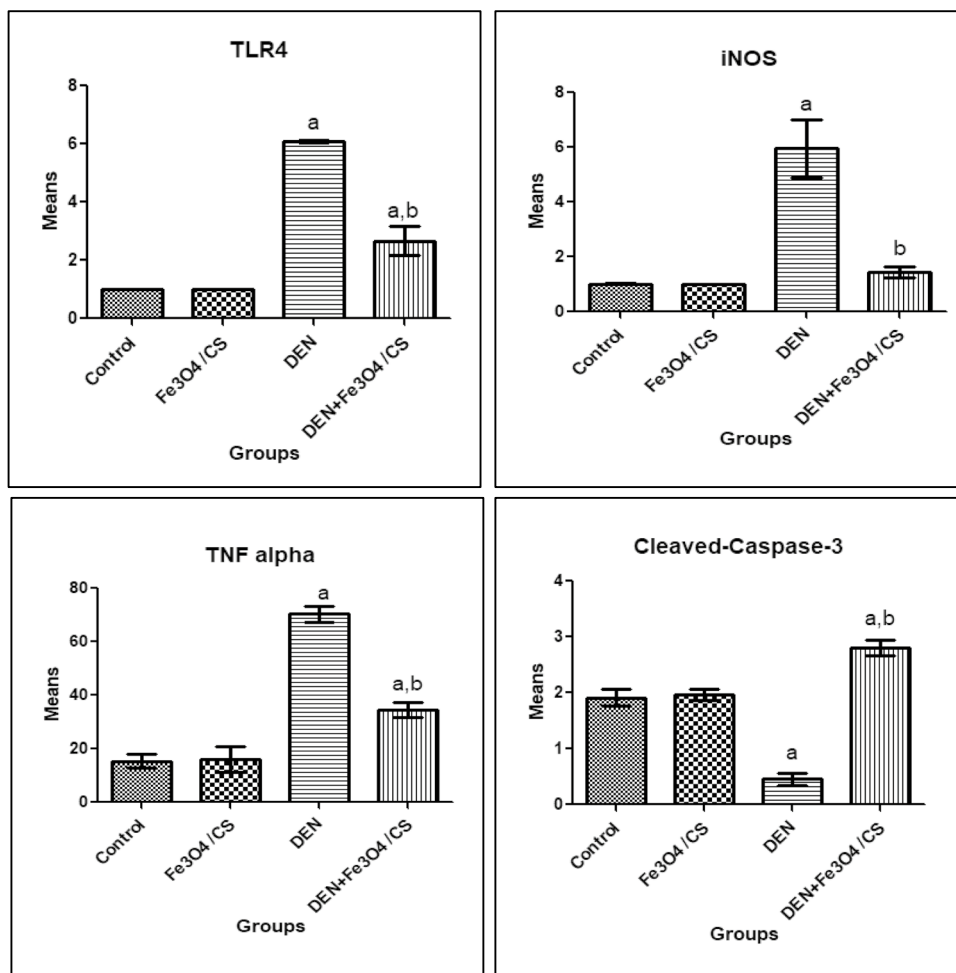
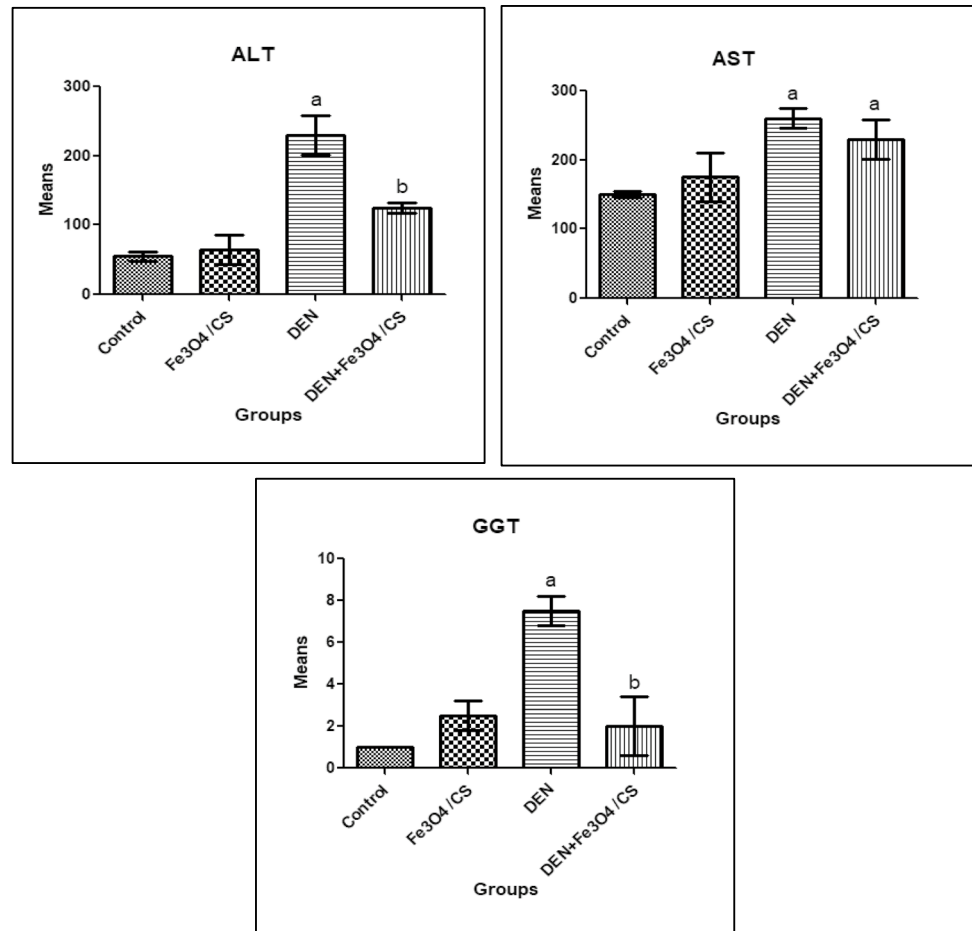


Fig. 5 The effect of $\text{Fe}_3\text{O}_4/\text{Cs}$ on liver function biomarkers. ^aSignificant difference versus control group at $P \leq 0.05$; ^bsignificant difference versus DEN group at $P \leq 0.05$



cytoplasm, as well as a few spaced hepatic sinusoids distributed in between the hepatic cords with fine Kupffer cell arrangement (Fig. 6a–b). Animals group treated with ($\text{Fe}_3\text{O}_4/\text{Cs}$) only showed normal histological picture similar to normal control group without any pathological alterations (Fig. 6c–d).

Histopathological alterations of liver tissue sections of hepatocellular carcinoma-induced rat group by (DEN) revealed polyhedral to round hepatocytes with dense, centrally located vesicular nuclei. The neoplastic areas showed poorly differentiated large cells with hyperchromatic nuclei and prominent nucleoli. The neoplastic cells showed pleomorphism, deeply basophilic scanty cytoplasm, and few mitotic figures (grade II). The hepatic lobule displayed disorganization of hepatic cords with hyperplasia of Kupffer cells (Fig. 6e–f).

Carcinogenic animals group treated by ($\text{Fe}_3\text{O}_4/\text{Cs}$) revealed necrobiotic changes of hepatic carcinoma cells with hyperplasia of Kupffer cells. Partial 51–99% tumor necrosis was noticed. Apoptosis and deeply eosinophilic cytoplasm without obvious mitotic figures were seen. Disorganization of carcinoma cells with widening of hepatic sinusoids were noticed. Leukocytic infiltration mainly lymphocytes and

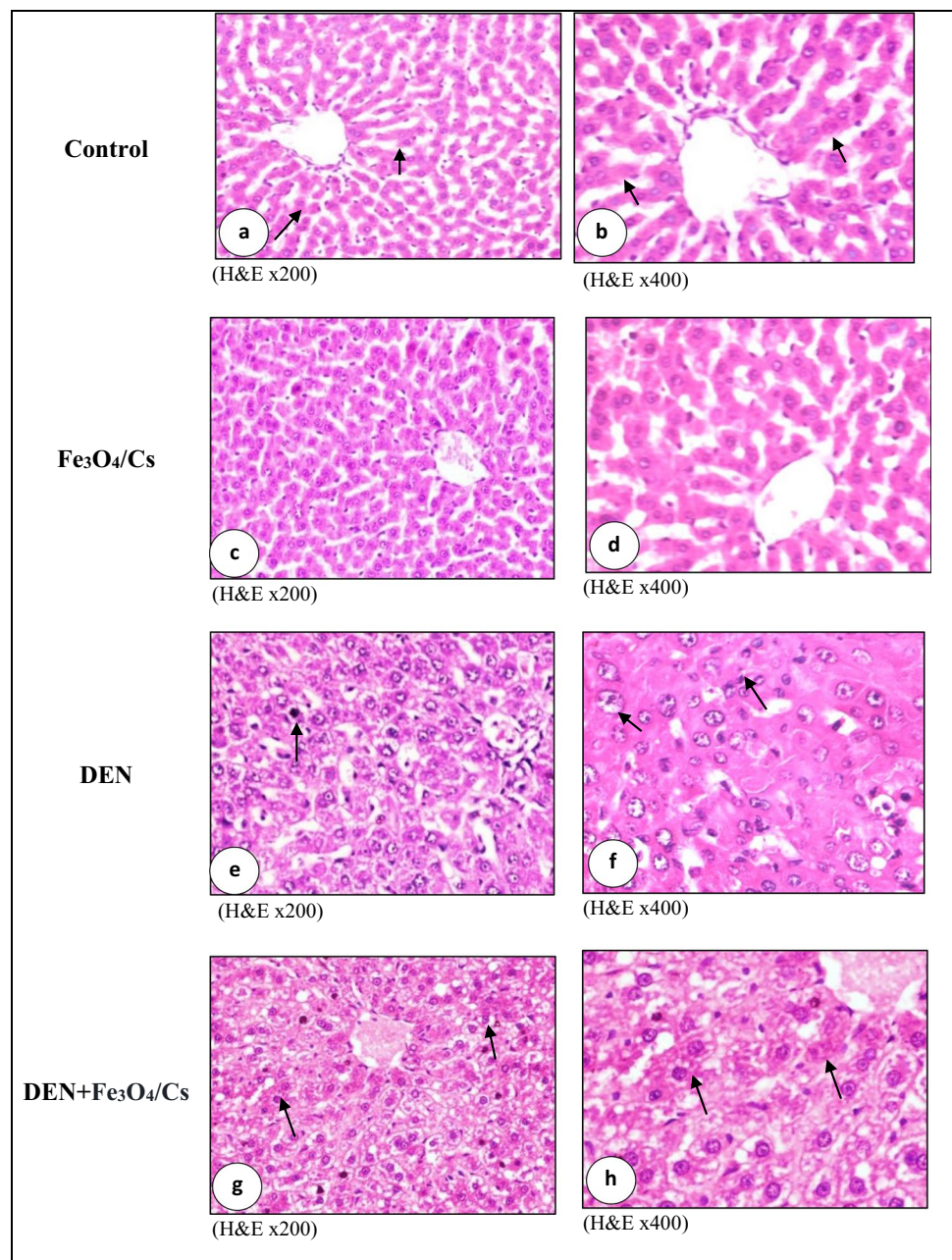
macrophages were seen. Numerous numbers of binucleated cells and karyomegaly with peripheral condensation of its chromatin were noticed (Fig. 6g–h).

Discussion

HCC is a worldwide issue. HCC is the sixth common cancer worldwide, while it is fourth common cancer in Egypt. Egypt is Africa's third and the world's 15th most populous country, for HCC [29]. Iron oxide nanoparticles possess hopes in nanomedicine because of their potential use in cancer therapy, drug transport, and bioimaging [30]. Because Fe_3O_4 nanoparticles are easy to combine and oxidize, they are frequently coated to achieve better characteristics for targeted drug/gene delivery [7]. In view of these considerations the aim of the current study was to prepare and evaluate the efficacy of $\text{Fe}_3\text{O}_4/\text{Cs}$ as an anticancer agent.

$\text{Fe}_3\text{O}_4/\text{Cs}$ were prepared by exposure to 20 kGy gamma radiation then characterized using TEM and XRD. Gamma radiation is favored method for metallic nanoparticles synthesis because it is reproducible, simple, inexpensive, and uses fewer toxic precursors, as well as may control the yield

Fig. 6 Photomicrograph of liver showing **a** normal histological structure of hepatic lobules arrow, **b** normal large polygonal cells with prominent round nuclei arrow, **c** normal histological structure of hepatic lobules, **d** normal large polygonal cells with prominent round nuclei, **e** deeply basophilic malignant cells with few mitotic figure arrow, **f** nuclear pleomorphism arrow and leukocytic infiltration, **g** necrobiotic changes of hepatic carcinoma cells with hyperplasia of Kupffer cells arrow, and **h** partial apoptosis and deeply eosinophilic cytoplasm without obvious mitotic figures arrow



shape of the monodispersed metallic nanoparticles [31]. Prepared $\text{Fe}_3\text{O}_4/\text{Cs}$ showed a typical TEM micrograph for monodispersed $\text{Fe}_3\text{O}_4/\text{chitosan}$ nanoparticles as chitosan inhibited the aggregation of nanoparticles. XRD showed characteristic peaks related to Fe_3O_4 nanoparticles (at 2-Theta: 35 °C, 42 °C, 58, and 63) and broad peak (in the 2-Theta range 20–30°) in related to the polymeric part of chitosan. The peak positions were unchanged, which illustrated that the chitosan binding process did not result in the phase change of Fe_3O_4 [32]. Prepared $\text{Fe}_3\text{O}_4/\text{Cs}$ were evaluated as anticancer agent for HCC DEN-induced rats, where PI3K/Akt/mTOR and MAPK (ERK, JNK, P38) signaling

pathways were studied, as well as inflammatory markers (TLR4, iNOS and $\text{TNF-}\alpha$), cleaved caspase-3, and liver enzyme (ALT, AST and GGT) activities.

The PI3K/AKT/mammalian target of rapamycin (mTOR) signalling pathway is one of the most essential intracellular pathways, and it can be regarded a key regulator for cancer [33]. PI3K/AKT/mTOR pathway activation leads to tumor growth and anticancer drug resistance [34]. Growth factors activate the PI3K/Akt/mTOR pathway by connecting to their receptors and activating the substrates of the receptors. The phosphoinositide 3-kinase (PI3K) then binds to the active receptor's intracellular part and transforms

phosphatidylinositol-4, 5-phosphate (PIP2) to phosphatidylinositol-3, 4, 5-phosphate (PIP3). PIP3 then stimulates the PDK1 to AKT pathway, causing mTOR to be activated [35]. PI3K/Akt/mTOR and MAPK are more frequently activated intracellular pathways and the best characterized in HCC. Possibly playing a role in its pathogenesis [36]. In the current study, the DEN-challenged group had higher levels of PI3K/Akt/mTOR and MAPK pathway expression. Previous studies had found similar findings [37, 38]. Nanoparticle-based mTOR targeted therapy appears to be a promising treatment option for a variety of malignancies [39]. It's worth mentioning that a large number of studies suggests that different NPs control mTOR activation, causing cell cycle arrest in cancerous cells [40], which simultaneously has an effect on the related signaling pathways AMPK and ERK. It is also worth noting that NP-mediated autophagy is correlated to the production of reactive oxygen species (ROS), which suppresses the mTOR pathway [41]. The Fe₃O₄ nanoparticles inhibited the mTOR phosphorylation [42] and AKT [43]. In the present study, Fe₃O₄/Cs modulated diethylnitrosamine (DEN)-induced HCC in animals models via PI3K/Akt/mTOR and MAPK (ERK, JNK, and P38) Signaling pathways. Such results were reported by the previous studies [41, 42, 44].

Toll-like receptor (TLR-4) appears to have a role in hepatocarcinogenesis, as TLR-4 expression increased as chronic hepatitis progressed to cirrhosis and then to HCC. TLR-4 expression was associated to a larger tumor size and a higher HCC grade, suggesting that it could be used to predict HCC prognosis. TLR-4 expression was found to be significantly higher in the DEN-treated group in the current investigation. Prior studies reported similar findings [45]. The effectiveness of metal oxide nanoparticles for TLRs varies depending on the metal type. Iron oxide nanoparticles (IONPs) differentially modulate TLR ligand-induced cytokine levels. The interactions between IONPs and TLR ligands are complicated and vary depending on the TLR ligand, nanoparticle size, and interactions between nanoparticles and TLR ligands [46]. Downstream TLR signaling causes MAPK cascades activation [47]. When these pathways are activated, macrophages undergo metabolic and functional changes, including differential expression of pro-inflammatory cytokines like tumor necrosis factor (TNF- α) [48]. In the current study, we observed upregulation in iNOS expression and increasing in TNF- α level in rats treated with DEN. Such results agree with the previous study done by Fathy and Nikaido, (2013) [49]. Metal oxide nanoparticles have been reported to induce both immunosuppressive and anti-inflammatory responses [50, 51]. According to the current findings, Fe₃O₄/Cs modulated the TLR4 activation. Also, Fe₃O₄/Cs treatment causes significant decreases in TNF- α level and downregulation in the expression of iNOS. Such results were reported by previous studies [46, 50, 52, 53].

Caspase-3 is a key molecule in cancer cell death. The active form of caspase-3, cleaved caspase-3, was the major cleavage enzyme that promoted apoptosis [54]. In the present study, we observed inhibition in cleaved caspase-3 activity in rats treated with DEN, which agree with the results reported by Lin et al. (2017) [55]. Fe₃O₄ nanoparticles induce apoptosis in cancer cells by raising the quantity of reactive oxygen species (ROS) and intracellular calcium, as well as boosting the expression of caspase-3 and caspase-9 and decreasing the expression of Bcl-2, as well as causing direct DNA damage [56]. The expression of cleaved caspase-3 is increased by the Fe₃O₄/Cs in the current study. Previous investigations had reported similar findings [57, 58].

Cytoplasmic transaminases, including ALT and AST, are released and circulated in response to DEN stimulation. Both ALT and AST are useful diagnostic markers for liver damage [59]. The data showed that the activities of ALT, AST, and GGT increased significantly, indicating that the DEN-induced HCC model was successfully constructed, as reported by the previous studies [37, 60, 61]. The present study demonstrated that Fe₃O₄/Cs treatment causes significant decreases in ALT, AST, and GGT levels. Also, inflammation response and pathological changes were alleviated by Fe₃O₄/Cs. Such results come in agreement with the previous studies [42, 62].

The present study concluded that administration of Fe₃O₄/Cs effectively inhibited the phosphorylations of PI3K/Akt/mTOR pathway and modulated P38, ERK, and JNK pathways. Moreover, it causes apoptosis in cancer cells by increasing the expression of cleaved caspase-3 and induces immunosuppression for cytokines. In addition, the inflammation response and pathological changes were alleviated by Fe₃O₄/Cs.

Acknowledgements We wish to thank Dr. Faten Ismail Abou El Fadl, Associate Professor of Polymer chemistry, Polymer Chemistry Department, National Center for Radiation Research and Technology, (NCRRT), Egyptian Atomic Energy Authority (EAEA), who helped us during preparation and characterization of chitosan-coated iron oxide nanocomposite (Fe₃O₄/Cs).

Funding Open access funding provided by The Science, Technology & Innovation Funding Authority (STDF) in cooperation with The Egyptian Knowledge Bank (EKB).

Data Availability The data presented in this study are available in this article.

Declarations

Ethics Approval All the ethical protocols for animal treatment were approved by the Ethical Committee at the National Center for Radiation Research and Technology (no: 3 A/ 22).

Conflict of Interest The authors declare no competing interests.

Open Access This article is licensed under a Creative Commons Attribution 4.0 International License, which permits use, sharing,

adaptation, distribution and reproduction in any medium or format, as long as you give appropriate credit to the original author(s) and the source, provide a link to the Creative Commons licence, and indicate if changes were made. The images or other third party material in this article are included in the article's Creative Commons licence, unless indicated otherwise in a credit line to the material. If material is not included in the article's Creative Commons licence and your intended use is not permitted by statutory regulation or exceeds the permitted use, you will need to obtain permission directly from the copyright holder. To view a copy of this licence, visit <http://creativecommons.org/licenses/by/4.0/>.

References

- Wang SZ, Lee SD, Sarkar D, Lee HM, Khan A, Bhati C, Levy MF (2021) Immunological characterization of hepatocellular carcinoma. *Hepatoma Res* 7
- Kim DW, Talati C, Kim R (2017) Hepatocellular carcinoma (HCC): beyond sorafenib—chemotherapy. *J Gastrointest Oncol* 8(2):256
- Singh K, Bhoori M, Kasu YA, Bhat G, Marar T (2018) Antioxidants as precision weapons in war against cancer chemotherapy induced toxicity—exploring the armoury of obscurity. *Saudi Pharm J* 26(2):177–190
- Cordani M, Somoza Á (2019) Targeting autophagy using metallic nanoparticles: a promising strategy for cancer treatment. *Cell Mol Life Sci* 76(7):1215–1242
- Xia L, Wang Y, Chen Y, Yan J, Hao F, Su X, Xu M (2017) Cuprous oxide nanoparticles inhibit the growth of cervical carcinoma by inducing autophagy. *Oncotarget* 8(37):61083
- Blanco J, Tomás-Hernández S, García T, Mulero M, Gómez M, Domingo JL, Sánchez DJ (2018) Oral exposure to silver nanoparticles increases oxidative stress markers in the liver of male rats and deregulates the insulin signalling pathway and p53 and cleaved caspase 3 protein expression. *Food Chem Toxicol* 115:398–404
- Shen T, Zhu W, Yang L, Liu L, Jin R, Duan J, Ai H (2018) Lactosylated N-Alkyl polyethylenimine coated iron oxide nanoparticles induced autophagy in mouse dendritic cells. *Regen Biomater* 5(3):141–149
- Chandrasekharan P, Tay ZW, Hensley D, Zhou XY, Fung BK, Colson C, Conolly S (2020) Using magnetic particle imaging systems to localize and guide magnetic hyperthermia treatment: tracers, hardware, and future medical applications. *Theranostics* 10(7):2965
- Hernández-Hernández AA, Aguirre-Álvarez G, Cariño-Cortés R, Mendoza-Huizar LH, Jiménez-Alvarado R (2020) Iron oxide nanoparticles: synthesis, functionalization, and applications in diagnosis and treatment of cancer. *Chem Pap* 74:3809–3824
- Reddy LH, Arias JL, Nicolas J, Couvreur P (2012) Magnetic nanoparticles: design and characterization, toxicity and biocompatibility, pharmaceutical and biomedical applications. *Chem Rev* 112(11):5818–5878
- Sang M, Luo R, Bai Y, Dou J, Zhang Z, Liu F, Liu W (2019) Mitochondrial membrane anchored photosensitive nano-device for lipid hydroperoxides burst and inducing ferroptosis to surmount therapy-resistant cancer. *Theranostics* 9(21):6209
- Alkhader E, Billa N, Roberts CJ (2017) Mucoadhesive chitosan-pectinate nanoparticles for the delivery of curcumin to the colon. *AAPS PharmSciTech* 18(4):1009–1018
- R Kamath P, Sunil D (2017) Nano-chitosan particles in anticancer drug delivery: an up-to-date review. *Mini Rev Med Chem* 17(15):1457–1487
- Ramasamy T, Tran TH, Cho HJ, Kim JH, Kim YI, Jeon JY, Kim JO (2014) Chitosan-based polyelectrolyte complexes as potential nanoparticulate carriers: physicochemical and biological characterization. *Pharm Res* 31(5):1302–1314
- Ramasamy T, Haidar ZS, Tran TH, Choi JY, Jeong JH, Shin BS, Kim JO (2014) Layer-by-layer assembly of liposomal nanoparticles with PEGylated polyelectrolytes enhances systemic delivery of multiple anticancer drugs. *Acta Biomater* 10(12):5116–5127
- Bharathi D, Ranjithkumar R, Vasantharaj S, Chandarshekar B, Bhuvaneshwari V (2019) Synthesis and characterization of chitosan/iron oxide nanocomposite for biomedical applications. *Int J Biol Macromol* 132:880–887
- Kim YC, Guan KL (2015) mTOR: a pharmacologic target for autophagy regulation. *J Clin Investig* 125(1):25–32
- Hosokawa N, Hara T, Kaizuka T, Kishi C, Takamura A, Miura Y, Mizushima N (2009) Nutrient-dependent mTORC1 association with the ULK1–Atg13–FIP200 complex required for autophagy. *Mol Biol Cell* 20(7):1981–1991
- Wang C, Cigliano A, Delogu S, Armbruster J, Dombrowski F, Evert M, Calvisi D (2013) Functional crosstalk between AKT/mTOR and Ras/MAPK pathways in hepatocarcinogenesis: implications for the treatment of human liver cancer. *Cell Cycle* 12(13):1999–2010
- Li L, Li L, Zhou X, Yu Y, Li Z, Zuo D, Wu Y (2019) Silver nanoparticles induce protective autophagy via Ca²⁺/CaMKK β /AMPK/mTOR pathway in SH-SY5Y cells and rat brains. *Nanotoxicology* 13(3):369–391
- Zeinali S, Nasirimoghaddam S, Sabbaghi S (2016) Investigation of the synthesis of chitosan coated iron oxide nanoparticles under different experimental conditions. *Int J Nanosci Nanotechnol* 12(3):183–190
- Wilbrandt W (1952) Behrens methods for calculation of LD50. *Arzneimittelforschung* 2(11):501–503
- Darwish HA, El-Boghdady NA (2013) Possible involvement of oxidative stress in diethylnitrosamine-induced hepatocarcinogenesis: chemopreventive effect of curcumin. *J Food Biochem* 37(3):353–361
- Khedri B, Shahanipour K, Fatahian S, Jafary F (2018) Preparation of chitosan-coated Fe₃O₄ nanoparticles and assessment of their effects on enzymatic antioxidant system as well as high-density lipoprotein/low-density lipoprotein lipoproteins on wistar rat. *Biomed Biotechnol Res J (BBRJ)* 2(1):68
- Bradford MM (1976) A rapid and sensitive method for the quantitation of microgram quantities of protein utilizing the principle of protein-dye binding. *Anal Biochem* 72(1–2):248–254
- Livak KJ, Schmittgen TD (2001) Analysis of relative gene expression data using real-time quantitative PCR and the 2⁻ $\Delta\Delta$ CT method. *Methods* 25(4) 402–408
- Bancroft JD, Stevens A, Turner DR (2013) Theory and practice of histological techniques, 4th edn. Churchill, Livingston, New York, London, San Francisco, Tokyo
- El-Gazzaz G, Sourianarayanan A, Menon KN, Sanabria J, Hashimoto K, Quintini C, Aucejo F (2013) Radiologic-histological correlation of hepatocellular carcinoma treated via pre-liver transplant locoregional therapies. *Hepatobiliary Pancreat Dis Int* 12(1):34–41
- Rashed WM, Kandeil MAM, Mahmoud MO, Ezzat S (2020) Hepatocellular carcinoma (HCC) in Egypt: a comprehensive overview. *J Egypt Natl Canc Inst* 32(1):1–11
- Geppert M, Himly M (2021) Iron oxide nanoparticles in bioimaging—an immune perspective. *Front Immunol* 12
- Cele T (2020) Preparation of nanoparticles. *Eng Nanomater-Health Saf IntechOpen*
- Unsoy G, Yalcin S, Khodadust R, Gunduz G, Gunduz U (2012) Synthesis optimization and characterization of chitosan-coated

- iron oxide nanoparticles produced for biomedical applications. *J Nanopart Res* 14(11):1–13
33. Yang J, Nie J, Ma X, Wei Y, Peng Y, Wei X (2019) Targeting PI3K in cancer: mechanisms and advances in clinical trials. *Mol Cancer* 18(1):1–28
 34. Martini M, De Santis MC, Braccini L, Gulluni F, Hirsch E (2014) PI3K/AKT signaling pathway and cancer: an updated review. *Ann Med* 46(6):372–383
 35. Geissler EK, Schlitt HJ, Thomas G (2008) mTOR, cancer and transplantation. *Am J Transplant* 8(11):2212–2218
 36. Finn RS (2013) Emerging targeted strategies in advanced hepatocellular carcinoma. *Sem Liver Dis* 33 S 01 S11–S19 Thieme Medical Publishers
 37. Guoyin Z, Hao P, Min L, Wei G, Zhe C, Changquan L (2017) Antihepatocarcinoma effect of *Portulaca oleracea* L. in mice by PI3K/Akt/mTOR and Nrf2/HO-1/NF- κ B pathway. *Evid-Based Complement Alternat Med* 2017
 38. Younis NS, Ghanim AM, Saber S (2019) Mebendazole augments sensitivity to sorafenib by targeting MAPK and BCL-2 signalling in n-nitrosodiethylamine-induced murine hepatocellular carcinoma. *Sci Rep* 9(1):1–16
 39. Lunova M, Smolková B, Lynnyk A, Uzhytchak M, Jirsa M, Kubinová Š, Lunov O (2019) Targeting the mTOR signaling pathway utilizing nanoparticles: a critical overview. *Cancers* 11(1):82
 40. Chiu HW, Xia T, Lee YH, Chen CW, Tsai JC, Wang YJ (2015) Cationic polystyrene nanospheres induce autophagic cell death through the induction of endoplasmic reticulum stress. *Nanoscale* 7(2):736–746
 41. Jia L, Hao SL, Yang WX (2020) Nanoparticles induce autophagy via mTOR pathway inhibition and reactive oxygen species generation. *Nanomedicine* 15(14):1419–1435
 42. Shen Y, Xiao Y, Zhang S, Wu S, Gao L, Shi S (2020) Fe₃O₄ nanoparticles attenuated *Salmonella* infection in chicken liver through reactive oxygen and autophagy via PI3K/Akt/mTOR signaling. *Front Physiol* 10:1580
 43. Shetake NG, Kumar A, Gaikwad S, Ray P, Desai S, Ningthoujam RS, Pandey BN (2015) Magnetic nanoparticle-mediated hyperthermia therapy induces tumour growth inhibition by apoptosis and Hsp90/AKT modulation. *Int J Hyperther* 31(8):909–919
 44. Park EJ, Umh HN, Kim SW, Cho MH, Kim JH, Kim Y (2014) ERK pathway is activated in bare-FeNPs-induced autophagy. *Arch Toxicol* 88(2):323–336
 45. El-Gendy E, Zakaria R, Abd Elsamee T, Agina H, El Badawy R (2021) Significance of toll-like receptor 4 (TLR4) & liver fatty acid-binding protein (L-FABP) expression in hepatocellular carcinoma an immunohistochemical study. *Benha Med J* 38(Academic issue):92–111
 46. Wolf-Grosse S, Mollnes TE, Ali S, Stenvik J, Nilsen AM (2018) Iron oxide nanoparticles enhance toll-like receptor-induced cytokines in a particle size- and actin-dependent manner in human blood. *Nanomedicine* 13(14):1773–1785
 47. Roy R, Singh SK, Das M, Tripathi A, Dwivedi PD (2014) Toll-like receptor 6 mediated inflammatory and functional responses of zinc oxide nanoparticles primed macrophages. *Immunology* 142(3):453–464
 48. Poon WL, Alenius H, Ndika J, Fortino V, Kolhinen V, Mešćeriakovas A, Karisola P (2017) Nano-sized zinc oxide and silver, but not titanium dioxide, induce innate and adaptive immunity and antiviral response in differentiated THP-1 cells. *Nanotoxicology* 11(7):936–951
 49. Fathy M, Nikaido T (2013) In vivo modulation of iNOS pathway in hepatocellular carcinoma by *Nigella sativa*. *Environ Health Prev Med* 18(5):377–385
 50. Shen CC, Liang HJ, Wang CC, Liao MH, Jan TR (2012) Iron oxide nanoparticles suppressed T helper 1 cell-mediated immunity in a murine model of delayed-type hypersensitivity. *Int J Nanomed* 7:2729
 51. Ngobili TA, Daniele MA (2016) Nanoparticles and direct immunosuppression. *Exp Biol Med* 241(10):1064–1073
 52. Grosse S, Stenvik J, Nilsen AM (2016) Iron oxide nanoparticles modulate lipopolysaccharide-induced inflammatory responses in primary human monocytes. *Int J Nanomed* 11:4625
 53. Lřšková S, Baliř P, Mičurová A, Kluknavský M, Okuliarová M, Puzserová A, Bernátová I (2020) Effect of iron oxide nanoparticles on vascular function and nitric oxide production in acute stress-exposed rats. *Physiol Res* 69(6)
 54. Asselin E, Mills GB, Tsang BK (2001) XIAP regulates Akt activity and caspase-3-dependent cleavage during cisplatin-induced apoptosis in human ovarian epithelial cancer cells. *Can Res* 61(5):1862–1868
 55. Lin B, Zhu M, Wang W, Li W, Dong X, Chen Y, Li M (2017) Structural basis for alpha fetoprotein-mediated inhibition of caspase-3 activity in hepatocellular carcinoma cells. *Int J Cancer* 141(7):1413–1421
 56. Ranjbary AG, Saleh GK, Azimi M (2021) Superparamagnetic iron oxide nanoparticles induce apoptosis in HT-29 cells by increasing ROS and damaging DNA
 57. Chauhan A, Kumar R, Singh P, Jha SK, Kuanr BK (2020) RF hyperthermia by encapsulated Fe₃O₄ nanoparticles induces cancer cell death via time-dependent caspase-3 activation. *Nanomedicine* 15(04):355–379
 58. Kasai S, Shimizu S, Tataru Y, Mimura J, Itoh K (2020) Regulation of Nrf2 by mitochondrial reactive oxygen species in physiology and pathology. *Biomolecules* 10(2):320
 59. Chen T, Gao J, Xiang P, Chen Y, Ji J, Xie P, Yan T (2015) Protective effect of platycodin D on liver injury in alloxan-induced diabetic mice via regulation of Treg/Th17 balance. *Int Immunopharmacol* 26(2):338–348
 60. Latief U, Husain H, Mukherjee D, Ahmad R (2016) Hepatoprotective efficacy of gallic acid during nitrosodiethylamine-induced liver inflammation in Wistar rats. *J Basic Appl Zool* 76:31–41
 61. Liao S, Liu J, Xu M, Zheng J (2018) Evaluation of the liver cancer prevention of anthocyanin extracts from mulberry (*Morus alba* L.) variety PR-01. *Adv Biosci Biotechnol* 9(09):423
 62. Ren Z, Chen X, Hong L, Zhao X, Cui G, Li A, Chen X (2020) Nanoparticle conjugation of ginsenoside Rg3 inhibits hepatocellular carcinoma development and metastasis. *Small* 16(2):1905233